High Strength, Ductile Braze Repairs for Stationary Gas Turbine Components—Part I

Both aviation and land based turbine components such as vanes/nozzles, combustion chambers, liners, and transition pieces often degrade and crack in service. Rather than replacing with new components, innovative repairs can help reduce overhaul and maintenance costs. These components are cast from either Co-based solid solution superalloys such as FSX-414 or Ni-based gamma prime precipitation strengthened superalloys such as IN738. The nominal compositions of FSX-414 and IN738 are Co–29.5Cr–10.5Ni–7W–2Fe [max]–0.25C–0.012B and Ni–0.001B–0.17C–8.5Co–16Cr–1.7Mo–3.4Al–2.6W–1.7Ta–2Nb–3.4Ti–0.1Zr, respectively. Diffusion brazing has been used for over 4 decades to repair cracks and degradation on these types of components. Typically, braze materials utilized for component repairs are Ni- and Co-based braze fillers containing B and/or Si as melting point depressants. Especially when repairing wide cracks typically found on industrial gas turbine components, these melting point depressants can form brittle intermetallic boride and silicide phases that affect mechanical properties such as low cycle and thermal fatigue. The objective of this work is to investigate and evaluate the use of hypereutectic Ni–Cr–Hf and Ni–Cr–Zr braze filler metals, where the melting point depressant is no longer B, but Hf and/or Zr. Typically, with joint gaps or crack widths less than 0.15 mm, the braze filler metal alone can be utilized. For cracks greater than 0.15 mm, a superalloy powder is mixed with the braze filler metal to enable wide cracks to be successfully brazed repaired. As a means of qualifying the diffusion braze repair, both metallurgical and mechanical property evaluations were carried out. The metallurgical evaluation consisted of optical and scanning electron microscopies, and microprobe analysis. The diffusion brazed area consisted of a fine-grained equiaxed structure with carbide phases, gamma (γ) dendrites, flower shaped/rosette gamma-gamma prime (γ-γ') eutectic phases, and Ni_7Hf_2, Ni_5HF, or Ni_5Zr intermetallic phases dispersed both intergranularly and intragranularly. Hardness tests showed that the Ni–Hf and Ni–Zr intermetallic phase only has a hardness range of 250–400 HV, whereas, the typical Cr-boride phases have hardness ranges from 800 HV to 1000 HV. Therefore the hardness values of the Ni–Hf and Ni–Zr intermetallic phases are 2.5–3.2 times softer than the Cr-boride intermetallic phases. As a result the low cycle fatigue (LCF) properties of the wide gap Ni–Cr–Hf and Ni–Cr–Zr brazed joints are superior to those of the Ni–Cr–B braze filler metals. The mechanical property evaluations were tensile tests at both room temperature and elevated temperature, stress rupture test from 760°C to 1093°C, and finally LCF tests, the latter being one of the most important and severe tests to conduct since the cracks being repaired are thermal fatigue driven. At the optimum braze thermal cycle, the mechanical test results achieved were a minimum of 80% and sometimes equivalent to that of the base metal properties. [DOI: 10.1115/1.3155397]

Warren Miglietti

Madeleine Du Toit
Associate Professor

Department of Materials Science and Metallurgical Engineering, University of Pretoria, Pretoria 0002, South Africa

1 Introduction

Over the past 2 decades, numerous technical papers have been published on a narrow gap (0.025–0.127 mm) and wide gap (greater than 0.127 mm) brazing for the manufacture [1–10] and repair [11–20] of nickel- and cobalt-based gas turbine engine components. In all these technical papers, the melt point depressant utilized was boron (B) and/or silicon (Si).

Examination of the binary phase diagrams with nickel as solvent revealed that hafnium (Hf) and zirconium (Zr) might be suitable for use as melting point depressants in novel braze filler metals for repairing Ni-base superalloy components. Nash and Nash [21] reported the existence of an invariant eutectic reaction in the Ni–Hf binary system at a composition of 30.5 wt % Hf and 69.5 wt % Ni (see Fig. 1). The eutectic temperature was quoted as 1190°C. Similarly, Nash and Jayanth [22] reported that the Ni–Zr binary system also contains a eutectic point located at 13 wt % Zr and 87 wt % Ni (see Fig. 2). The eutectic temperature was quoted as 1170°C. In order to determine whether Hf and Zr can be used as melting point depressants in Ni-base braze filler metals, Ni and Cr powders were mixed with Hf or Zr powder to make up the simple tertiary braze compositions.

Upon determining that a Ni–Cr–Hf or Ni–Cr–Zr braze can indeed be utilized to join two Ni-base superalloys together, these braze alloys were mixed with a superalloy powder to determine if wide gap brazed joints can be produced.

The objectives of this research work are as follows.

- Demonstrate that the two hypereutectic braze alloys consisting of Ni–Cr–Hf and Ni–Cr–Zr can successfully melt and flow like typical braze alloys used in the aerospace industry or industrial gas turbine (IGT) industry.

Contributed by the International Gas Turbine Institute of ASME for publication in the JOURNAL OF ENGINEERING FOR GAS TURBINES AND POWER. Manuscript received April 10, 2008; final manuscript received May 4, 2008; published online May 11, 2010. Review conducted by Dilip R. Ballal. Paper presented at the ASME Turbo Expo 2008: Land, Sea and Air (GT2008), Berlin, Germany, June 9–13, 2008.

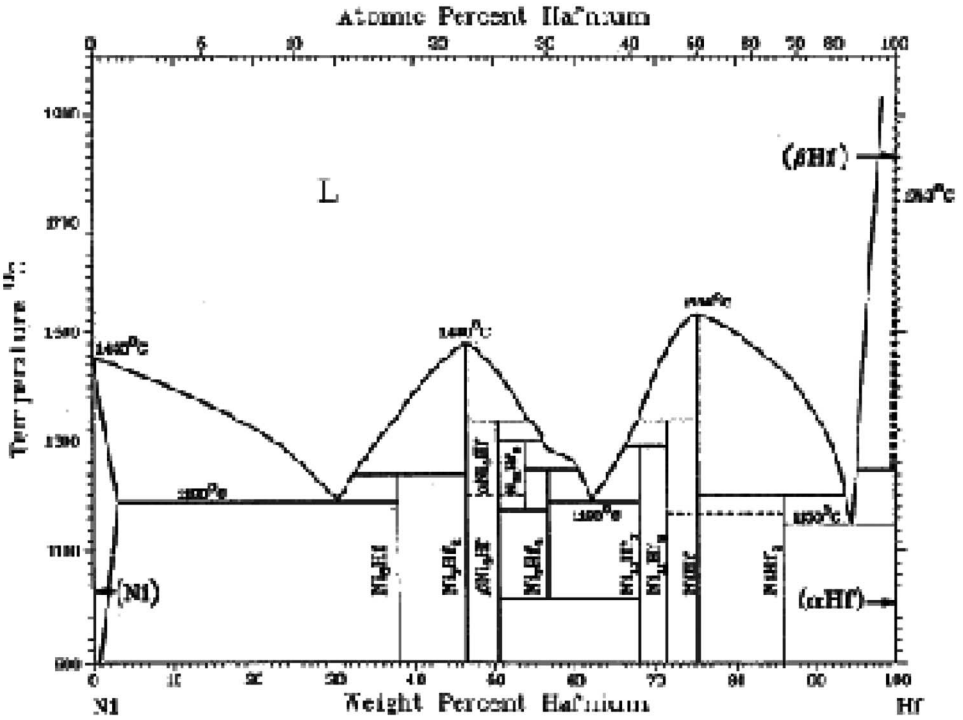

Fig. 1 Binary Ni–Hf phase diagram

- Determine the microstructure of the two braze joints and quantitatively and qualitatively analyze the resultant intermetallic phases formed in the joint. Only optical and scanning electron microscopy (SEM) work will be documented in this paper, whereas microprobe results will be documented in a subsequent paper.
- Demonstrate that the two braze alloys consisting of Ni–Cr–Hf and Ni–Cr–Zr can successfully be used in combina-

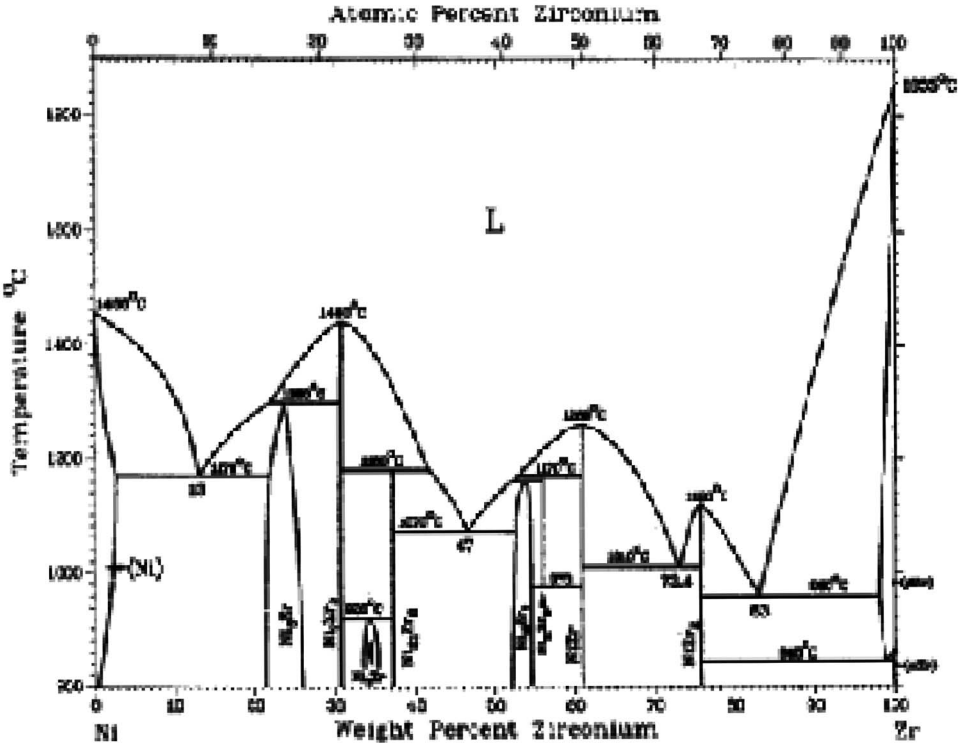

Fig. 2 Binary Ni–Zr phase diagram

tion with a Ni-based superalloy powder MarM247 (Ni–0.001B–0.15C–10Co–8.25Cr–1.5Hf–0.7Mo–5.5Al–10W–3Ta–1Ti–0.05Zr–0.5Fe) as part of the wide gap diffusion brazing process.
- Evaluate the tensile, creep rupture, and low cycle fatigue properties of the wide gap braze joints; the latter results, which will be documented in a subsequent paper.

2 Experimental Procedure

2.1 Metallurgical Evaluation. Inconel 738 (abbreviated as IN738 throughout this work) flat plates of composition Ni–0.001B–0.17C–8.5Co–16Cr–1.7Mo–3.4Al–2.6W–1.7Ta–2Nb–3.4Ti–0.1Zr were excised from the roots of scrap blades by electrical discharge machining (EDM). The root of a blade is not exposed to any appreciable temperature and stress in service; hence, material taken from this area is normally referred to as virginlike as-cast material. After the EDM process, the material was ground down in a surface grinder to 2 mm thickness with various lengths and widths. These plates were subsequently cleaned by grit blasting with 220 grit silicon carbide media. The plates were then wiped with acetone to remove the residue left over from the grit blasting. The hypereutectic Ni–Cr–Hf and/or Ni–Cr–Zr braze alloy in powder form was mixed with a binder to form a paste. After the acetone evaporated, either a layer of Ni–Cr–Hf or Ni–Cr–Zr braze alloy (by itself or mixed with the MarM247 powder) in paste form was applied over the IN738 plate or between two IN738 plates (like a filling in a sandwich). The samples, where the Ni–Cr–Hf braze alloy was used, and the other samples, where the Ni–Cr–Zr braze alloy was used, were allowed to dry in air for 1 h before a vacuum heat treat in a laboratory furnace with a maximum temperature capability of 1300°C. Because the furnace does not have quench capability, the samples were slowly cooled (furnace cooled) to room temperature.

The vacuum cycle used was as follows.

(1) Ramp up at a rate of 15°F/min minimum to a temperature of 450°C.
(2) Hold at 450°C for 20 min to let the binder burn off/burn away.
(3) Ramp up at a rate of 15°F/min minimum to a temperature of 1150°C.
(4) Hold at 1150°C for 20 min to let the samples stabilize at this temperature.
(5) Ramp up at a rate of 15°F/min minimum to a temperature of 1238°C to get the braze alloy to melt and flow. Note that a proprietary homogenization heat treatment was given to the IN738 material prior to brazing to prevent incipient melting during the braze thermal cycle.
(6) Hold at the temperatures in (5) above for times varying from 40 min to 24 h.
(7) Furnace cool to room temperature.

After exposing the samples to a vacuum braze cycle as mentioned above, the samples were sectioned and mounted using conventional metallographic practices. The metallographic mounts were etched with Marble's reagent to reveal the microstructure. Optical and SEMs were performed. The optical microscope was a Nikon Epiphot 200 model, with a maximum magnification capability of 1000×. The SEM instrument was a JEOL-Oxford model, using the ZAF software correction. The acceleration voltage was 20 kV, the % dead time was approximately 50 s, the sample tilt angle was 0 deg, and the acquisition time was 150 s.

2.2 Tensile and Creep Rupture Tests. Tensile tests at 22°C and elevated temperatures of 650°C, 760°C, 870°C, and 980°C were performed. MarM247 specimens of composition Ni–0.001B–0.15C–10Co–8.25Cr–1.5Hf–0.7Mo–5.5Al–10W–3Ta–1Ti–0.05Zr–0.5Fe were joined together at 1238°C for times varying from 40 min to 24 h; however, only results for brazed joints

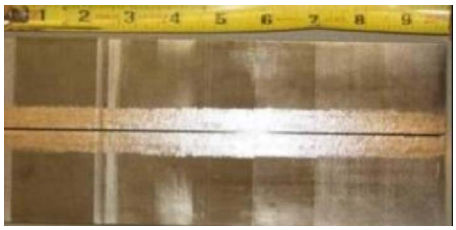

Fig. 3 Plate of 247.7 mm length with 1.5 mm groove machined in the center

produced up to 12 h will be reported here (the tensile test results of brazed joints produced at a time of 24 h will be reported in a subsequent paper). Unlike the metallographic samples, these tensile test samples were age heat treated at 870°C for 20 h, typical of the age heat treat performed during repair. Cast plates of either MarM247 or IN738 material of dimensions 247.7mm long, 127 mm wide, and 15.24 mm thick were obtained, as seen in Fig. 3. A 1.5 mm groove was machined along the length, in the middle of the plate, as seen in Fig. 4, to simulate the typical larger crack width found in IGT stationary nozzles, as opposed to generally smaller crack widths typically found in aircraft gas turbine nozzles/vanes.

After machining, the groove was cleaned by grit blasting with 220 grit silicon carbide media. After all the braze and thermal processing, tensile and stress rupture specimens were excised from the plate via EDM. Threads were machined on either ends of the specimens, and the gauge length reduced in diameter so that the brazed joint was a full butt joint in the center/middle of the test specimen, as seen in Fig. 5.

Creep rupture tests were conducted, as shown in Table 1. IN738 specimens were joined together at 1238°C for 12 h, similar to the method described for tensile testing. As a result the creep rupture test specimens were also prepared in a butt joint configuration, as seen in Fig. 5, with the 1.5 mm wide gap braze joint being in the center of the gauge length, to simulate a typical crack width found in an IGT engine operated nozzle segment, as seen in Fig. 6.

The objective of these creep rupture tests is to get an initial idea of the creep rupture properties of the MarM247/Ni–Cr–Zr and MarM247/Ni–Cr–Hf braze formulations. As a reminder the creep rupture properties of the joint will be really determined by the MarM247 powder in addition to the Ni–Cr–Zr or Ni–Cr–Hf braze

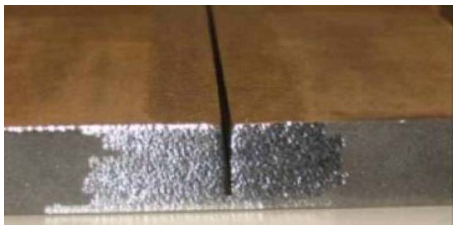

Fig. 4 1.5 mm groove machined down the center/middle of the plate

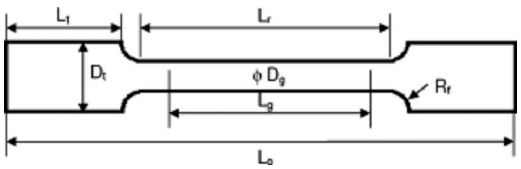

Fig. 5 Configuration of tensile and creep rupture test specimens

Table 1 Creep rupture test conditions

Temperature (°C)	Stress level (MPa)		
	1	2	3
843	345	276	228
982	138	104	76

filler metal. The intermetallic phases that formed in the brazed joint will determine its ductility, i.e., the elongation and RA values.

3 Metallurgical and Mechanical Test Results

3.1 Metallurgical Results and Discussion

3.1.1 Hypereutectic Ni–Cr–Hf Brazed Joints. Figure 7 shows a micrograph of the narrow gap, Ni–Cr–Hf brazed joint consisting of gamma (γ) dendrites, flower shaped gamma-gamma prime (γ-γ') eutectic phases, and Ni_7Hf_2 intermetallic phases. Two phases were analyzed in the Ni–Cr–Hf narrow gap brazed joints, shown in Fig. 8. One phase analyzed was the γ dendrites or γ phase because the energy dispersive X-ray analysis revealed a composition of 78.72Ni–5.97Co–4.47Cr–4.00Al–2.82W–2.53Fe–0.53Mo–0.38Ti. All values are in wt %. The second phase analyzed was the Ni_7Hf_2 intermetallic phase. The composition revealed was 49.21Ni–45.74Hf–2.32W–1.94Co–0.37Cr–0.28Al–0.14Ti. Once again all values are in wt %. Nash and Nash [21] reported that the Ni_7Hf_2 intermetallic phase contains 46.5% Hf, whereas the Ni_5Hf phase contains 37.9% Hf. Therefore it appears that the Ni_7Hf_2 intermetallic phase existed in these joints and contains essentially Ni and Hf, but W, Co, Cr, Al, and Ti are soluble in this phase to a small extent.

Figure 9 shows the microstructure of a wide gap brazed joint, where a superalloy powder MarM247 was mixed with the Ni–Cr–Hf braze filler metal. The joint is composed of a majority of the prior Ni-base superalloy powder particles, eutectic phases, Ni_7Hf_2 intermetallic phases, and a thick layer of γ dendrites/phases that are bonding/sintering the Ni-base superalloy powder particles together.

Fig. 6 1.5 mm wide cracks on the sidewalls of a typically industrial gas turbine nozzle segment

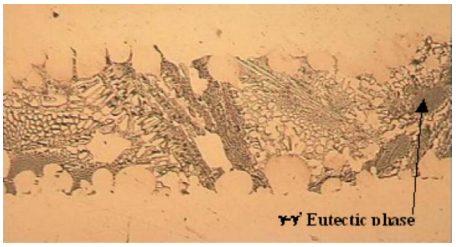

Fig. 7 Microstructure of a Ni–Cr–Hf narrow gap brazed joint produced at 1238°C/18 h (magnification of 200×)

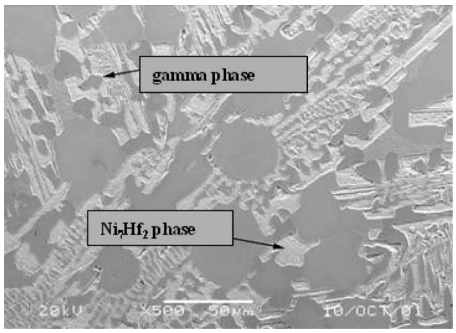

Fig. 8 Scanning electron micrograph of the Ni–Cr–Hf brazed joint

Two phases were analyzed in the wide gap brazed joint shown in Fig. 10, where the MarM247 superalloy powder was mixed with the Ni–Cr–Hf braze filler metal. One phase analyzed was the γ dendrites or γ phase because the energy dispersive X-ray analysis revealed a composition of 78.06Ni–6.68Co–3.74Cr–4.22Al–2.42W–3.01Fe–0.79Mo–0.81Ti–0.27Zr. All values are in wt %. The second phase analyzed was the Ni_7Hf_2 intermetallic phase. The composition revealed was 50.31Ni–43.93Hf–2.32W–2.50Co–0.40Cr–0.39Al–0.14Ti. Once again all values are in wt %. Nash and Nash [21] reported that the Ni_7Hf_2 intermetallic phase contains 46.5% Hf, whereas the Ni_5Hf phase contains 37.9% Hf. Therefore it appears that the Ni_7Hf_2 intermetallic phase that existed here contains essentially Ni and Hf, but W, Co, Cr, Al and Ti are soluble in this phase to a small extent.

Figure 11 shows the microstructure of a wide gap brazed joint

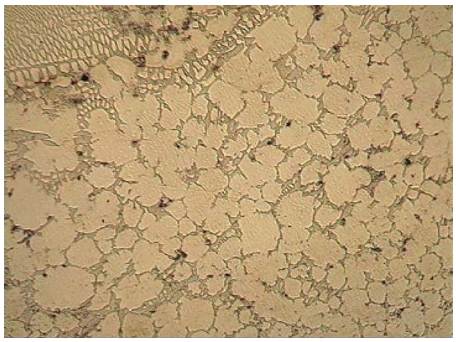

Fig. 9 Microstructure of MarM247 superalloy powder mixed with the Ni–Cr–Hf braze produced at 1238°C for 40 min (magnification of 200×)

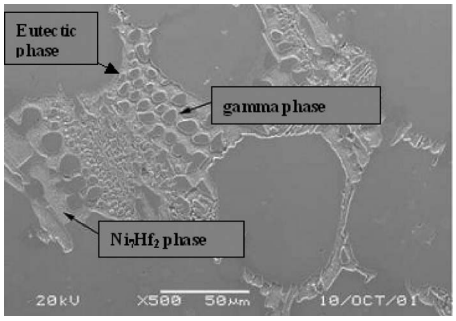

Fig. 10 Scanning electron micrograph of the wide gap brazed joint produced at 1238°C/40 min by mixing MarM247 powder and a Ni–Cr–Hf braze filler metal

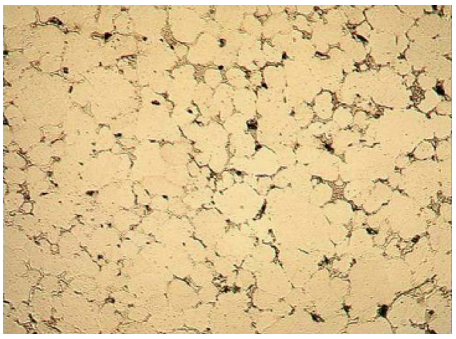

Fig. 11 Microstructure of MarM247 superalloy powder mixed with the Ni–Cr–Hf braze produced at 1238°C for 4 h (magnification of 200×)

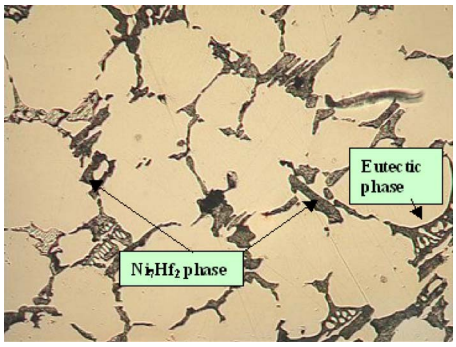

Fig. 13 Microstructure of MarM247 superalloy powder mixed with the Ni–Cr–Hf braze produced at 1238°C for 12 h +1232°C for 4 h SHT (magnification of 200×)

produced at 1238°C for 4 h. The joint is composed of a majority of the prior superalloy powder particles, eutectic and Ni_7Hf_2 intermetallic phases, and a thin layer of γ dendrites/phases that are bonding/sintering the Ni-base superalloy powder particles together. Two phases were analyzed in the wide gap brazed joints produced at 1238°C for 4 h, as seen in Fig. 12. One phase analyzed was the γ dendrites or γ phase because the energy dispersive X-ray analysis revealed a composition of 75.27Ni–6.26Co–6.88Cr–3.67Al–2.29W–2.22Fe–1.93Mo–0.73Ti–0.74Zr. All values are in wt %. The second phase analyzed was the Ni_7Hf_2 intermetallic phase. The composition revealed was 49.50Ni–46.56Hf–1.36W–2.01Co–0.38Cr–0.19Ti. Once again all values are in wt %. Nash and Nash [21] reported that the Ni_7Hf_2 intermetallic phase contains 46.5% Hf, whereas the Ni_5Hf phase contains 37.9% Hf. Therefore it appears that the Ni_7Hf_2 intermetallic phase found here contains essentially Ni and Hf, but W, Co, Cr, and Ti are soluble in this phase to a small extent.

Figure 13 shows the microstructure of a wide gap brazed joint produced at 1238°C for 12 h, followed by a 1232°C for 4 h solution heat treatment (SHT). Percentage wise, the joint is composed of a majority of the MarM247 powder particles, eutectic phases (γ phase+Ni_7Hf_2 phase), plus solid Ni_7Hf_2 intermetallic phases that are left at the grain boundaries. One would then expect from this joint that the properties would approach that of the MarM247 superalloy, rather than the Ni–Cr–Hf braze alloy.

Figure 14 is a microstructure taken in the SEM, of the phases in the Ni–Cr–Hf wide gap brazed joint, produced at 1238°C for 12 h+4 h SHT at 1232°C. The intermetallic phase analyzed revealed a composition of 53.01Ni–43.09Hf–2.43Co–0.82Cr–0.20Ti–0.45W. Once again all values are in wt %. Nash and Nash [21] reported that the Ni_7Hf_2 intermetallic phase contains 46.5% Hf, whereas the Ni_5Hf phase contains 37.9% Hf. Therefore it appears that the intermetallic phase analyzed here was indeed the Ni_7Hf_2 phase containing essentially Ni and Hf, but W, Co, Cr, and Ti are soluble in this phase to a small extent.

Note that optical and SEMs of brazed Ni–Cr–Hf joints produced at 1238°C for 18 h and 24 h, respectively, will be reported in a subsequent paper.

3.1.2 Hypereutectic Ni–Cr–Zr Brazed Joints. Figure 15 shows a micrograph of the Ni–Cr–Zr brazed joint consisting of γ dendrites and eutectic and Ni_5Zr intermetallic phases. Two phases were also analyzed in the Ni–Cr–Zr narrow gap brazed joints shown in Fig. 16. One phase analyzed was the γ dendrites or γ phase because the energy dispersive X-ray analysis revealed a composition of 78.82Ni–9.00Zr–3.08Co–2.97Cr–3.05Al–1.24Fe–1.57Mo–0.26Ti. All values are in wt %. The second phase analyzed was the Ni_5Zr intermetallic phase. The composition revealed was 71.24Ni–24.91Zr–1.45W–1.47Co–0.57Cr–0.38Mo. Once again all values are in wt %. Nash and Jayanth [22] reported that the Ni_7Zr_2 intermetallic phase contains 30.75% Zr, whereas the Ni_5Zr phase contains 21.32–25.95% Zr. Therefore it appears

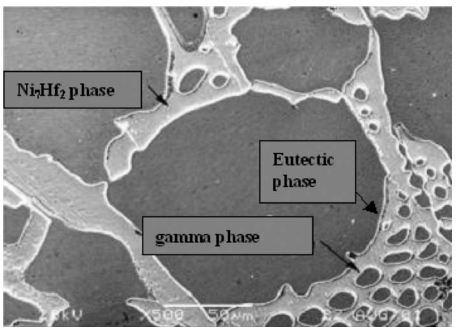

Fig. 12 Scanning electron micrograph of the wide gap brazed joint produced at 1238°C/4 h by mixing MarM247 powder and a Ni–Cr–Hf braze filler metal

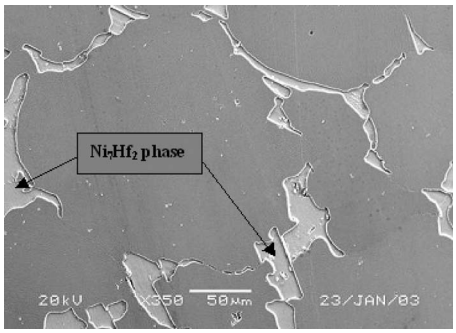

Fig. 14 Scanning electron micrograph of the wide gap brazed joint produced at 1238°C for 12 h+1232°C for 4 h SHT by mixing MarM247 powder and a Ni–Cr–Hf braze filler metal

Fig. 15 Microstructure of a Ni–Cr–Zr narrow gap brazed joint produced at 1238°C/18 h (magnification of 200×)

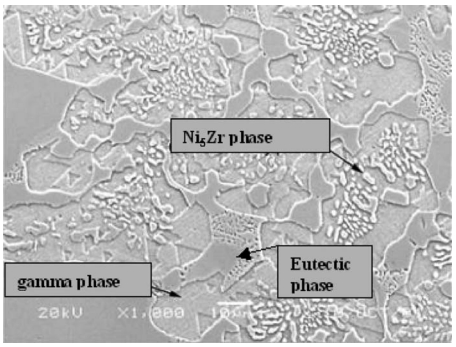

Fig. 16 Scanning electron micrograph of the Ni–Cr–Zr brazed joint

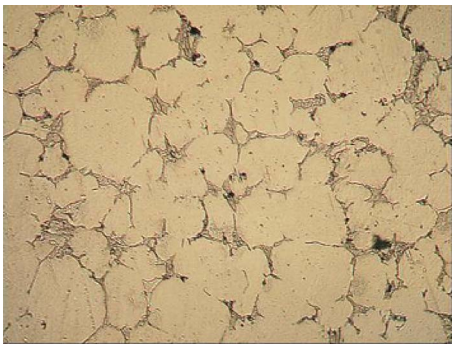

Fig. 19 Microstructure of MarM247 superalloy powder mixed with the Ni–Cr–Zr braze produced at 1238°C for 4 h (magnification of 200×)

that the Ni_5Zr intermetallic phase existed in these joints and thus contains essentially Ni and Zr, but W, Co, Cr, and Mo are soluble in this phase to a small extent.

Figure 17 shows the microstructure of a wide gap brazed joint produced at 1238°C for 40 min, where the MarM247 powder was mixed with the Ni–Cr–Zr braze filler metal. The joint is composed of a majority of the prior superalloy powder particles, eutectic and Ni_5Zr intermetallic phases, and a thick layer of γ dendrites/phases that are bonding/sintering the Ni-base superalloy powder particles together.

Two phases were analyzed in the wide gap brazed joint shown in Fig. 18, where the MarM247 superalloy powder was mixed with the Ni–Cr–Zr braze filler metal. One phase analyzed was the γ dendrites or γ phase because the energy dispersive X-ray analysis revealed a composition of 74.48Ni–8.76Zr–5.64Co–3.21Cr–3.27Al–2.26W–1.86Mo–0.52Ti. All values are in wt %. The second phase analyzed was the Ni_5Zr intermetallic phase. The composition revealed was 69.49Ni–24.24Zr–2.03W–2.99Co–0.62Cr–0.41Mo–0.21Ti. Once again all values are in wt %. Nash and Jayanth [22] reported that the Ni_7Zr_2 intermetallic phase contains 30.75% Zr, whereas the Ni_5Zr phase contains 21.32–25.95% Zr. Therefore it appears that the Ni_5Zr intermetallic phase existed in these joints and thus contains essentially Ni and Zr, but W, Co, Cr, and Mo are soluble in this phase to a small extent.

Figure 19 shows the microstructure of a wide gap brazed joint produced at 1238°C for 4 h. The joint is composed of a majority of the prior superalloy powder particles, eutectic and Ni_5Zr intermetallic phases, and a thin layer of γ dendrites/phases that are bonding/sintering the superalloy powder particles together. Two phases were analyzed in the wide gap brazed joint produced at 1238°C for 4 h, as shown in Fig. 20. One phase analyzed was the γ dendrites or γ phase because the energy dispersive X-ray analysis revealed a composition of 79.54Ni–5.90Co–5.34Cr–3.98Al–1.81W–11.11Fe–0.85Mo–0.64Ti–0.83Zr. All values are in wt %. The second phase analyzed was the Ni_5Zr intermetallic phase. The composition revealed was 71.35Ni–24.47Zr–0.70W–2.28Co–0.61Cr–0.16Mo–0.43Al. Once again all values are in wt %. Nash and Jayanth [22] also reported that the Ni_7Zr_2 intermetallic phase contains 30.75% Zr, whereas the Ni_5Zr phase contains 21.32–25.95% Zr. Therefore it appears that the Ni_5Zr intermetallic phase existed in these joints and thus contains essentially Ni and Zr, but W, Co, Cr, Mo, and Al are soluble in this phase to a small extent.

Figure 21 shows the microstructure of a wide gap brazed joint produced at 1238°C for 12 h, followed by 1232°C for 4 h SHT. Percentage wise, the joint is composed of a majority of the MarM247 powder particles, eutectic phases (γ phase+Ni_7Zr phase), plus solid Ni_7Zr intermetallic phases that are left at the grain boundaries. One would then expect from this joint that the

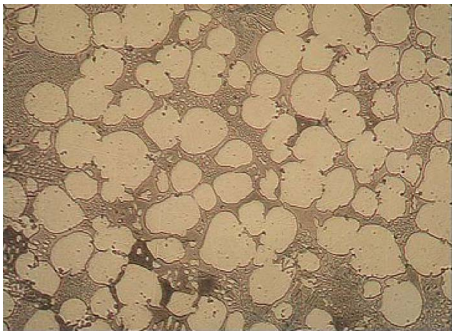

Fig. 17 Microstructure of MarM247 superalloy powder mixed with the Ni–Cr–Zr braze produced at 1238°C for 40 min (magnification of 200×)

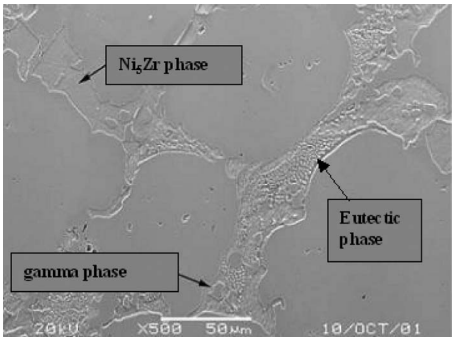

Fig. 18 Scanning electron micrograph of the wide gap brazed joint produced by mixing MarM247 superalloy powder and a Ni–Cr–Zr braze filler metal

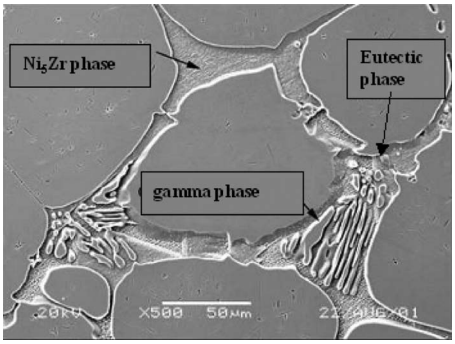

Fig. 20 Scanning electron micrograph of the wide gap brazed joint produced at 1238°C/4 h by mixing MarM247 powder and a Ni–Cr–Zr braze filler metal

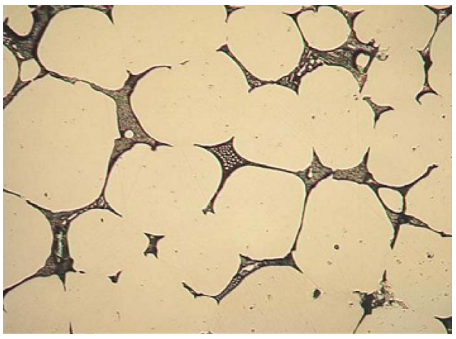

Fig. 21 Microstructure of MarM247 superalloy powder mixed with the Ni–Cr–Zr braze produced at 1238°C/12 h +1232°C/4 h SHT (magnification of 200×)

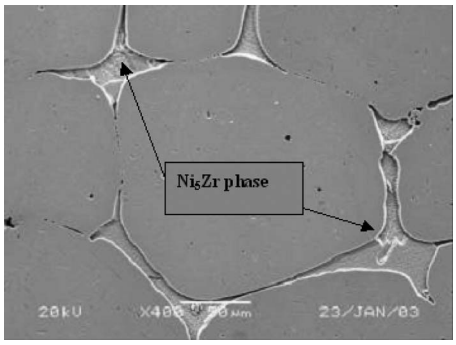

Fig. 22 Scanning electron micrograph of the wide gap brazed joint produced at 1238°C for 12 h+1232°C for 4 h SHT by mixing MarM247 powder and a Ni–Cr–Zr braze filler metal

properties would approach that of the MarM247 superalloy, rather than the Ni–Cr–Zr braze alloy. Figure 22 is a microstructure also taken from the SEM of the phases in the Ni–Cr–Zr wide gap brazed joint produced at 1238°C for 12 h+4 h SHT at 1232°C. The intermetallic phase analyzed revealed a composition of 70.78Ni–25.44Zr–2.27Co–0.81Cr–0.44Al–0.25W. Nash and Jayanth [22] also reported that the Ni_7Zr_2 intermetallic phase contains 30.75% Zr, whereas the Ni_5Zr phase contains 21.32–25.95% Zr. Therefore it appears that the Ni_5Zr intermetallic phase existed in these joints and thus contains essentially Ni and Zr, but W, Co, Cr, and Al are soluble in this phase to a small extent. Note that optical and SEMs of Ni–Cr–Zr brazed joints produced at 1238°C for 18 h and 24 h, respectively, will be reported in a subsequent report.

3.2 Tensile Test Results and Discussion. Tables 2–6 show the tensile test results of the wide gap brazed joints (MarM247 +Ni−Cr−Hf/Zr braze) at various temperatures. All test results are an average of three specimens. In addition UTS is the ultimate tensile strength, YS is the yield strength, Elong is the elongation, and RA is the reduction in area.

As seen in Table 2, room temperature tensile and yield strengths of the Ni–Cr–Hf joints, produced at 1238°C for 40 min, are 34% and 30%, respectively, of the MarM247 base metal properties, whereas the tensile and yield strengths of the Ni–Cr–Zr joints, produced at 1238°C for 40 min, are 58% and 63%, respectively, of the MarM247 base metal properties. Hence, it would appear that for short processing times (40 min), the Ni–Cr–Hf joints are considerably weaker than the Ni–Cr–Zr joints. However, the Ni–Cr–Hf joints have slightly greater than half the ductility, i.e., ±60% of the MarM247 base metal, whereas the Ni–Cr–Zr joints have only about ±40%. Hence it would appear that the joints containing the Ni–Cr–Hf intermetallic phases are softer and more ductile compared with the joints containing the Ni–Cr–Zr intermetallic phases.

Table 2 Tensile results at 22°C of the brazed specimens

Tensile properties	Ni–Cr–Hf joints 1238°C for 40 min	Ni–Cr–Zr joints 1238°C for 40 min	Ni–Cr–Hf joints 1238°C for 4 h	Ni–Cr–Zr joints 1238°C for 4 h	MarM247 base metal
UTS (MPa)	323	557	344	564	960
YS (MPa)	239	505	302	74.0	800
Elong (%)	4.7	3.0	2.7	3.0	7.9
RA (%)	6.3	4.4	3.9	4.5	10.0

Table 3 Tensile results at 650°C of the brazed specimens

Tensile properties	Ni–Cr–Hf joints 1238°C for 40 min	Ni–Cr–Zr joints 1238°C for 40 min	Ni–Cr–Hf joints 1238°C for 4 h	Ni–Cr–Zr joints 1238°C for 4 h	MarM247 base metal
UTS (MPa)	343	562	408	569	1040
YS (MPa)	265	513	308	501	805
Elong (%)	2.8	2.2	3.1	2.3	7.0
RA (%)	3.6	2.9	3.8	2.9	9.7

Table 4 Tensile results at 760°C of the brazed specimens

Tensile properties	Ni–Cr–Hf joints 1238°C for 40 min	Ni–Cr–Zr joints 1238°C for 40 min	Ni–Cr–Hf joints 1238°C for 4 h	Ni–Cr–Zr joints 1238°C for 4 h	MarM247 base metal
UTS (MPa)	333	593	464	602	1000
YS (MPa)	282	553	380	524	815
Elong (%)	2.5	1.2	2.9	2.2	6.0
RA (%)	3.2	5.9	3.0	4.3	8.4

Table 5 Tensile results at 870°C of the brazed specimens

Tensile properties	Ni–Cr–Hf joints 1238°C for 40 min	Ni–Cr–Zr joints 1238°C for 40 min	Ni–Cr–Hf joints 1238°C for 4 h	Ni–Cr–Zr joints 1238°C for 4 h	MarM247 base metal
UTS (MPa)	289	444	342	480	790
YS (MPa)	211	414	277	404	650
Elong (%)	2.0	1.0	2.2	2.1	5.0
RA (%)	3.0	2.4	3.2	3.1	7.7

Therefore, for short processing times, the ductility of the Ni–Cr–Zr and Ni–Cr–Hf brazed joints appears greater than the ductility of the joints produced which have B as the melting point depressant. References for ductility values of wide gap braze joints using B as a melt point depressant are available in Refs. [23–25]. Typically joints produced for short processing times with B as the melt point depressant have only ductility values in the range of 0.5–1.0%. Hence it would appear that the Ni–Hf and Ni–Zr intermetallic phases in the wide gap brazed joint contribute to enhanced ductility compared with brazed joints having Cr–B or Ni–B intermetallic phases present.

As also seen in Table 2, room temperature tensile and yield strengths of the Ni–Cr–Hf joints, produced at 1238°C for 4 h, are 36% and 38%, respectively, of the MarM247 base metal properties, whereas the tensile and yield strengths of the Ni–Cr–Zr joints, produced at 1238°C, are 59% and 64%, respectively, of the MarM247 base metal properties. Hence it would appear that for processing times of 4 h, the Ni–Cr–Hf joints are considerably weaker than the Ni–Cr–Zr joints. In addition, the increase in processing time, from 40 min to 4 h, resulted in a decrease in the ductility of the Ni–Cr–Hf joints from ±60% of the MarM247 base metal ductility to 36% of the base metal ductility. However, the ductility of Ni–Cr–Zr joints stayed the same even though the processing time was increased from 40 min to 4 h and was about ±40% of the base metal ductility. Hence it would appear that after increasing the processing time from 40 min to 4 h, the brazed joints containing the Ni–Cr–Hf intermetallic phases are harder and more brittle in comparison to the brazed joints containing the Ni–Cr–Zr intermetallic phases. Nevertheless, these data provide initial evidence that if higher joint strengths can be achieved by processing for even longer times, while maintaining similar levels of ductility, the use of the Zr and/or Hf as a melting point depressant in lieu of B may prove a great benefit for crack repair on IGT components.

As seen in Table 3, at 650°C, the tensile and yield strengths of the Ni–Cr–Hf joints, produced at 1238°C for 40 min, are both 33% of the MarM247 base metal properties, whereas the tensile and yield strengths of the Ni–Cr–Zr joints are 54% and 64%, respectively, of the MarM247 base metal properties. Processing at 1238°C for 4 h resulted in the tensile and yield strengths of the Ni–Cr–Hf joints, having 39% and 38%, respectively, of the base metal properties, whereas the tensile and yield strengths of the Ni–Cr–Zr joints have 55% and 62%, respectively, of the MarM247 base metal properties. Hence, as also seen in Table 2, it would appear that for processing times of 4 h and less, the Ni–Cr–Hf joints are considerably weaker than the Ni–Cr–Zr joints. However, the Ni–Cr–Hf joints produced at 1238°C for 40 min have approximately 40% of the ductility of the MarM247 base metal, whereas the Ni–Cr–Zr joints have only about ±32% of the ductility of the MarM247 base metal. The Ni–Cr–Hf joints produced at 1238°C for 4 h have approximately 42% of the ductility of the MarM247 base metal, whereas the Ni–Cr–Zr joints have only about ±31% of the ductility of the MarM247 base metal. Therefore it would appear that at 650°C, the joints containing the Ni–Hf intermetallic phases are softer and ductile than the joints containing the Ni–Zr intermetallic phases.

As seen in Table 4, at 760°C, the tensile and yield strengths of the Ni–Cr–Hf joints, produced at 1238°C for 40 min, are 33% and 35%, respectively, of the MarM247 base metal properties, whereas the tensile and yield strengths of the Ni–Cr–Zr joints are 59% and 68%, respectively, of the MarM247 base metal properties. The tensile and yield strengths of the Ni–Cr–Hf joints, produced at 1238°C for 4 h, are 46% and 47%, respectively, of the MarM247 base metal properties, whereas the tensile and yield strengths of the Ni–Cr–Zr joints are 60% and 64%, respectively, of the MarM247 base metal properties. Hence, as also seen in Tables 2 and 3, it would appear that for processing times of 4 h and less, the Ni–Cr–Hf joints are considerably weaker than the Ni–Cr–Zr joints. However, the Ni–Cr–Hf joints produced at 1238°C for 40 min have approximately 42% of the ductility of the MarM247 base metal, whereas the Ni–Cr–Zr joints have only about ±20% of the ductility of the MarM247 base metal. The Ni–Cr–Hf joints produced at 1238°C for 4 h have approximately 42% of the ductility of the MarM247 base metal, and similarly, the Ni–Cr–Zr joints have about ±42% of the ductility of the MarM247 base metal. Therefore it would appear that at 760°C, for the joints produced for 4 h, the joints containing the Ni–Hf intermetallic phases have equivalent softness and ductility compared with the joints containing the Ni–Zr intermetallic phases.

As seen in Table 5, at 870°C, the tensile and yield strengths of the Ni–Cr–Hf joints, produced at 1238°C for 40 min, are 36% and 32%, respectively, of the MarM247 base metal properties, whereas the tensile and yield strengths of the Ni–Cr–Zr joints are 56% and 64%, respectively, of the MarM247 base metal properties. The tensile and yield strengths of the Ni–Cr–Hf joints, produced at 1238°C for 4 h, are 43% and 43%, respectively, of the MarM247 base metal properties, whereas the tensile and yield

Table 6 Tensile results at 980°C of the brazed specimens

Tensile properties	Ni–Cr–Hf joints 1238°C for 40 min	Ni–Cr–Zr joints 1238°C for 40 min	Ni–Cr–Hf joints 1238°C for 4 h	Ni–Cr–Zr joints 1238°C for 4 h	MarM247 base metal
UTS (MPa)	195	261	266	308	506
YS (MPa)	141	245	206	214	312
Elong (%)	1.8	0.8	2.7	3.1	4.7
RA (%)	2.9	1.9	3.1	6.2	7.5

Note: The tensile test results for the Ni–Cr–Zr brazed joints produced at 1238°C for 12 h and 24 h, respectively, will be reported in a subsequent paper.

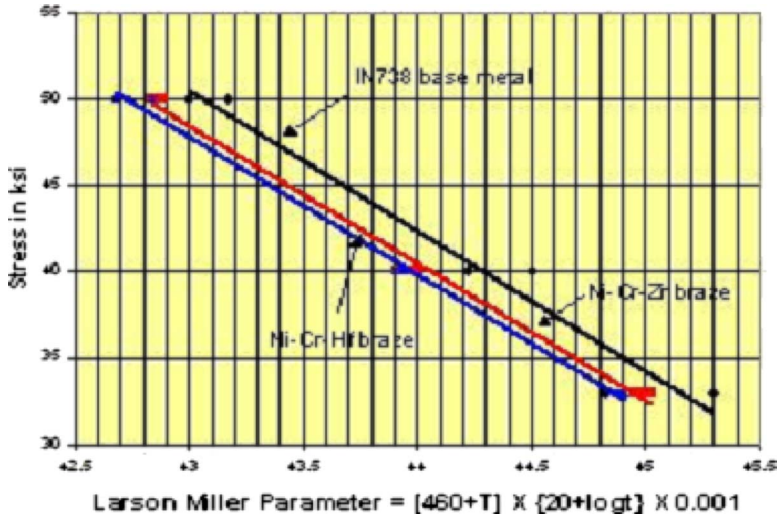

Fig. 23 Larson–Miller plot of the two brazed joints tested at 843°C at various stresses/loads

strengths of the Ni–Cr–Zr joints are 61% and 62%, respectively, of the MarM247 base metal properties. Hence, as also seen in Tables 2–4, it would appear that for processing times of 4 h and less, the Ni–Cr–Hf joints are considerably weaker than the Ni–Cr–Zr joints. However, the Ni–Cr–Hf joints produced at 1238°C for 40 min have approximately 40% of the ductility of the MarM247 base metal, whereas the Ni–Cr–Zr joints have only about ±20% of the ductility of the MarM247 base metal. The Ni–Cr–Hf joints produced at 1238°C for 4 h have approximately 43% of the ductility of the MarM247 base metal, whereas the Ni–Cr–Zr joints have approximately ±42% of the ductility of the MarM247 base metal. Therefore it would appear that at 870°C, the joints produced for 4 h, containing the Ni–Hf intermetallic phases, have equivalent softness and ductility compared with the joints containing the Ni–Zr intermetallic phases.

Finally, as seen in Table 6, at 980°C, the tensile and yield strengths of the Ni–Cr–Hf joints, produced at 1238°C for 40 min, are 39% and 45%, respectively, of the MarM247 base metal properties, whereas the tensile and yield strengths of the Ni–Cr–Zr joints are 52% and 79%, respectively, of the MarM247 base metal properties. The tensile and yield strengths of the Ni–Cr–Hf joints, produced at 1238°C for 4 h, are 53% and 66%, respectively, of the MarM247 base metal properties, whereas the tensile and yield strengths of the Ni–Cr–Zr joints are 61% and 69%, respectively, of the MarM247 base metal properties. Hence, as also seen in Tables 2–5, it would appear that for processing times of 4 h and less, the Ni–Cr–Hf joints are considerably weaker than the Ni–Cr–Zr joints. However, the Ni–Cr–Hf joints produced at 1238°C for 40 min have approximately 38% of the ductility of the MarM247 base metal, whereas the Ni–Cr–Zr joints have only about ±17% of the ductility of the MarM247 base metal. The Ni–Cr–Hf joints produced at 1238°C for 4 h have approximately 50% of the ductility of the MarM247 base metal, whereas the Ni–Cr–Zr joints have ±74% of the ductility of the MarM247 base metal. Therefore for the first time at an elevated temperature of 980°C, joints produced for 4 h, containing the Ni–Zr intermetallic phases, are softer and more ductile compared with the joints containing the Ni–Hf intermetallic phases.

3.3 Creep Rupture Results and Discussion. Brazed joints for creep rupture testing were produced at 1238°C for 12 h followed by a 1232°C for 4 h SHT.

The creep rupture properties of the Ni–Cr–Zr brazed joints at 843°C/345 MPa are 77.0% of the IN738 base metal properties, whereas the Ni–Cr–Hf brazed joints are 67.9% of the IN738 base metal properties. Similarly, at 843°C/276 MPa, the Ni–Cr–Zr brazed joints are 62.8% of the IN738 base metal properties, whereas the Ni–Cr–Hf brazed joints are 59.7% of the IN738 base metal properties. At 843°C/228 MPa, the Ni–Cr–Zr brazed joints are 88.8% of the IN738 base metal properties, whereas the Ni–Cr–Hf brazed joints are 79.0% of the IN738 base metal properties.

Figure 23 shows the creep rupture results of both braze materials on a Larson–Miller plot. This shows that the Ni–Cr–Zr braze joints have superior creep rupture properties (10% superior) when compared with the Ni–Cr–Hf brazed joints. In spite of the inferior creep rupture properties of the Ni–Cr–Hf brazed joints compared with the Ni–Cr–Zr joints, the ductility of the former braze joints is superior to that of the latter brazed joints. The average Elong and RA of the Ni–Cr–Hf brazed joints are 77% and 85% of the base metal values, respectively, whereas the average Elong and RA of the Ni–Cr–Zr brazed joints are 70% and 75% of the base metal values, respectively. This implies that the joints containing the Ni–Hf intermetallic phases are more ductile than the joints containing the Ni–Zr intermetallic phases, and in turn both are thrice as ductile as the joints containing brittle boride phases.

The creep rupture properties of the Ni–Cr–Zr brazed joints at 982°C/138 MPa are 77.8% of the IN738 base metal properties, whereas the Ni–Cr–Hf brazed joints are 64.0% of the IN738 base metal properties. Similarly at 982°C/104 MPa the Ni–Cr–Zr brazed joints are 70.0% of the IN738 base metal properties, whereas the Ni–Cr–Hf brazed joints are 60.9% of the IN738 base metal properties. At 982°C/76 MPa, the Ni–Cr–Zr brazed joints are 81.2% of the IN738 base metal properties, whereas the Ni–Cr–Hf brazed joints are 78.3% of the IN738 base metal properties.

Figure 24 shows the creep rupture results of both braze materials on a Larson–Miller plot. This shows that the Ni–Cr–Zr braze joints have superior creep rupture properties (8.7% superior) when compared with the Ni–Cr–Hf brazed joints.

In spite of the inferior creep rupture properties of the Ni–Cr–Hf brazed joints compared with the Ni–Cr–Zr joints, the ductility of the former braze joints is superior to that of the latter brazed joints. The average Elong and RA of the Ni–Cr–Hf brazed joints are 73% and 70% of the base metal values, respectively, whereas the average Elong and RA of the Ni–Cr–Zr brazed joints are 60% and 60% of the base metal values, respectively. This implies that the joints containing the Ni–Hf intermetallic phases are more ductile than the joints containing the Ni–Zr intermetallic phases, and in turn both are thrice as ductile as the joints containing brittle boride phases.

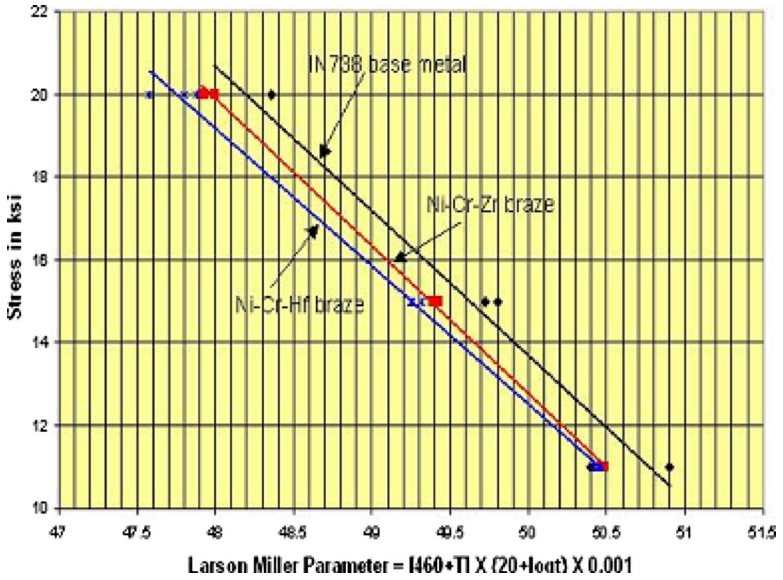

Fig. 24 Larson–Miller plot of the two brazed joints tested at 982°C at various stresses/loads

Typically, the average Elong values and RA values of brazed joints, with B as a melting point depressant that form boride phases, are 1–3% and 1–3%, respectively, whereas the Elong and RA values of the Ni–Cr–Zr and Ni–Cr–Hf joints range from 4% to 6% and 5–9%, respectively.

Figures 23 and 24 show the Larson–Miller plots at each individual test temperature; however, since Larson–Miller is a plot of both temperature (T) and time (t) on the x-axis, all the creep rupture data produced in this work can be plotted on one graph to get a total overall indication. As can be seen in Fig. 25, one can rank the three materials in descending order of creep rupture strength, viz., IN738 base metal, MarM247/Ni–Cr–Zr, and MarM247/Ni–Cr–Hf. The Larson–Miller plot can be divided into three regions: a high stress, low temperature region, an intermediate stress, intermediate temperature region, and a low stress, high temperature region. It is important to evaluate the properties at all three conditions since actual nozzle segments operate in all three regimes during engine service.

These creep rupture samples were not age heat treated at 1121°C for 2 h+843°C for 24 h, typical of what would occur, when a component is repaired. Nevertheless, these data still provide a relevant comparison between the Ni–Cr–Zr and Ni–Cr–Hf braze joints. Since the material is tested in the solution heat treated condition, one would expect the material to be annealed (soft) and exhibit enhanced ductility and reduced creep rupture strength. Therefore, the absolute creep rupture properties of the joints are expected to improve after the age heat treatment but the ductility marginally decreased. In this solution heat treated condition, the creep rupture properties of the Ni–Cr–Hf and Ni–Cr–Zr joints are between 65% and 75% of the IN738 base metal properties. Typically, based on past experience, with brazed joints using a Ni–B system, the age heat treatment will produce an increase in creep rupture properties of 15–20%. Therefore, if these

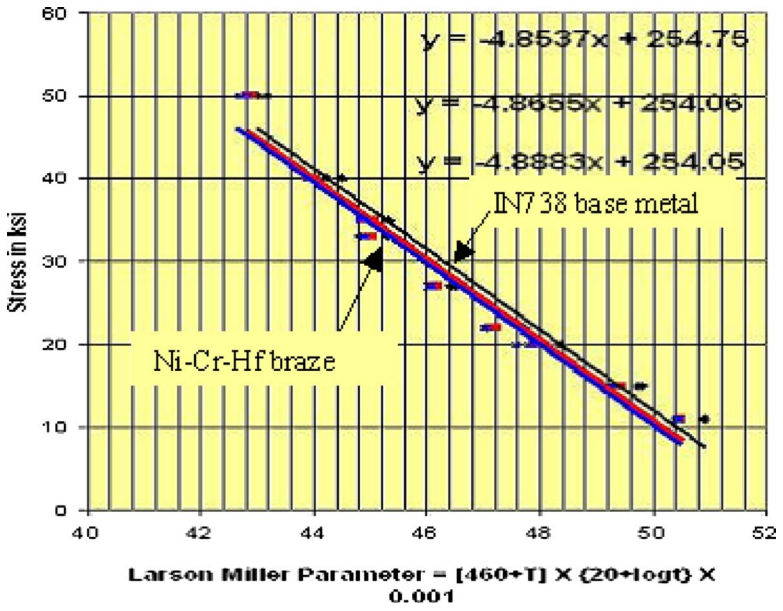

Fig. 25 Larson–Miller plot of the IN738 base metal versus the two brazed joints

samples were age heat treated, the properties of the Ni–Cr–Zr and Ni–Cr–Hf joints are expected to increase to 80–90% of the base metal properties.

4 Conclusions

IN738 or MarM247 can be joined together using either one of the two braze alloys developed. The joints produced at 1238°C for 40 min or 18 h consisted of a dendritic structure, gamma (γ) dendrites, flower shaped gamma-gamma prime (γ-γ') eutectic phases, and Ni_7Hf_2 intermetallic phases or Ni_5Zr intermetallic phases.

A reasonably dense, low porosity wide gap brazed joint, consisting of a two-phase microstructure, with the original Ni-base superalloy powder particles surrounded or engulfed with either the original Ni–Cr–Hf or the Ni–Cr–Zr braze alloy existed after processing at 1238°C for 40 min. Ni_5Zr or Ni_7Hf_2 intermetallic phases occurred intergranularly, and γ dendrites/phases existed as thick films engulfing the original Ni-base superalloy powder particles.

A dense, low porosity joint processed at 1238°C for 4 h consisted of a two-phase microstructure with coarse and fine grains. The γ dendrites/phases and Ni_5Zr or Ni_7Hf_2 phases existed intergranularly.

The major difference between the joints produced at 1238°C for 40 min and 4 h was the reduction in the amount or volume fraction of the γ dendrites/phases and Ni_5Zr or Ni_7Hf_2 phases. Unlike the thick films that existed in the joints produced at 1238°C for 40 min, the joints produced at 1238°C for 4 h showed that in many areas, no continuous films appeared. In fact, in many areas, only isolated and discrete γ dendrites/phases and Ni_5Zr or Ni_7Hf_2 phases existed.

A dense, low porosity joint processed at 1238°C for 12 h, followed by a solution heat treatment of 1232°C for 4 h, consisted of a two-phase microstructure with coarse and fine grains. Intermetallic phases existed intergranularly, and these were determined to be either Ni_7Hf_2 or Ni_5Zr phases.

The major difference between the joints produced at 1238°C for 12 h and the joints produced at 1238°C for 4 h was the reduction in the amount or volume fraction of the γ phases and Ni_5Zr or Ni_7Hf_2 intermetallic phases.

At all tensile test temperatures from 22°C to 980°C, the tensile and yield strengths of the Ni–Cr–Zr joints, produced either at 1238°C for 40 min or 4 h, are superior to those of the Ni–Cr–Hf joints.

Typically the tensile and yield strengths of the Ni–Cr–Hf joints, produced at 1238°C for 40 min, are only 30–40% of the MarM247 base metal properties (depending on the test temperature), whereas the tensile and yield strengths of the Ni–Cr–Zr joints are only 52–62% of the MarM247 base metal properties. Hence for short processing times of 40 min, the Ni–Cr–Zr joints have superior strength than the Ni–Cr–Hf joints.

Typically the tensile and yield strengths of the Ni–Cr–Hf joints, produced at 1238°C for 4 h, are only 36–66% of the MarM247 base metal properties (depending on the test temperature), whereas the tensile and yield strengths of the Ni–Cr–Zr joints are only 55–70% of the MarM247 base metal properties. Hence for processing times of 4 h, the Ni–Cr–Zr joints have superior strength when compared with the Ni–Cr–Hf joints. Consistently, an increase in processing time from 40 min to 4 h resulted in an increase in the tensile and yield strengths of both the Ni–Cr–Hf and Ni–Cr–Zr joints.

The Ni–Cr–Hf joints produced at 1238°C for 40 min have superior ductility when compared with the Ni–Cr–Zr joints. Depending on the testing temperature, the Ni–Cr–Hf joints have ductility in the order of 38–60% of the MarM247 base metal, whereas the Ni–Cr–Zr joints have ductility in the order of 17–40% of the MarM247 base metal. This would imply that the joints containing the Ni–Cr–Hf intermetallic phases are softer and more ductile when compared with the joints containing the Ni–Cr–Zr intermetallic phases. Intermetallic phases are usually hard and brittle, so having a "more ductile" intermetallic phase is quite a contradiction in terms.

The Ni–Cr–Hf joints produced at 1238°C for 4 h generally have superior ductility, except at 980°C, when compared with the Ni–Cr–Zr joints. Depending on the testing temperature, the Ni–Cr–Hf joints have ductility in the order of 36–50% of the MarM247 base metal, whereas the Ni–Cr–Zr joints have ductility in the order of 31–74% of the MarM247 base metal. These data imply that the joints containing the Ni–Hf intermetallic phases are softer and more ductile when compared with the joints containing the Ni–Zr intermetallic phases. At 980°C, the trend is opposite, where the Ni–Cr–Zr joints have very good ductility of ±74% of the base metal value. This ductility level is the highest achieved to date in this study. Consistently, an increase in processing time from 40 min to 4 h resulted in an increase in the ductility of the Ni–Cr–Zr joints.

Creep rupture tests performed at temperatures of 860°C and 982°C indicated that the Ni–Cr–Zr brazed joints had superior properties to that of the Ni–Cr–Hf joints, i.e., between 7% and 10%. Of more importance were the ductility measurements in the form of Elong % and RA %. These data showed that the Ni–Cr–Hf brazed joints were 19–13% more ductile than the Ni–Cr–Zr brazed joints. These results are consistent with the tensile data, which showed the same trend.

5 Preface for a Future Technical Publication

This extensive research has spanned a 5 year time period, making it difficult to provide a comprehensive summary in a short technical paper. As a result, a subsequent paper will follow that includes metallurgical results as well as tensile, creep test, and LCF results of joints brazed at 1238°C for 12 h and 24 h. In addition, the microstructures of various hypo- and hypereutectic braze compositions developed will be described.

Acknowledgment

Thanks to Professor Madeleine Du Toit (my supervisor) for her thoughtful guidance throughout this work.

References

[1] Lugscheider, E., and Kim, D. S., 1991, "New Low-Melting Nickel-Based High Temperature Brazing Alloys," Schweissen Schneiden, **43**(4), pp. 222–226.

[2] Lugscheider, E., and Partz, K. D., 1983, "High Temperature Brazing of Stainless Steel With Nickel-Base Filler Metals BNi-2, BNi-5, and BNi-7," Weld. J. (Miami, FL, U.S.), June, pp. 160s–164s.

[3] Sakamoto, A., Fujiwara, C., Hattori, T., and Sakai, S., 1989, "Optimizing Processing Variables in High Temperature Brazing, With Nickel-Based Filler Metals," Weld. J. (Miami, FL, U.S.), March, pp. 63–71.

[4] Draugelates, U., and Hartmann, K. H., 1978, "Behaviour of Brazed Nickel Alloy Under Cyclic and Thermal Load," Weld. J. (Miami, FL, U.S.), October, pp. 298s–302s.

[5] Tung, S., Lim, L., and Lai, M., 1996, "Solidification Phenomena in Nickel Base Brazes Containing Boron and Silicon," Scr. Mater., **34**(5), pp. 763–769.

[6] Gale, W., and Wallach, R., 1991, "Influence of Isothermal Solidification on Microstructural Development in Ni-Si-B Filler Metals," Mater. Sci. Technol., **7**, pp. 1143–1148.

[7] Wu, W., Chandel, R., Seow, H., and Li, H., 2001, "Wide Gap Brazing of Stainless Steel to Nickel Base Superalloy," J. Mater. Process. Technol., **113**, pp. 215–221.

[8] Tung, S., Lim, L., and Lai, M., 1995, "Microstructural Evolution and Control in BNi-4 Brazed Joints of Nickel 270," Scr. Metall. Mater., **33**(8), pp. 1253–1259.

[9] Leone, E., Rabinkin, A., and Sarna, B., 2006, "Microstructure of Thin Gauge Austenitic and Ferritic Stainless Steel Joints Brazed With Metglas Amorphous Foils," Weld. World, doc 1713-05/I-1147–041.

[10] Miyazawa, Y., and Ariga, T., 1993, "A Study of the Brazeability of Nickel Based Brazing Filler Metal Foils for Joining Nickel Base Metal to Mild Steel Base Metal," Weld. J. (Miami, FL, U.S.), July, pp. 294s–300s.

[11] Huang, X., Yandt, S., Nagy, D., and Yao, M., 2007, "Effect of Ruthenium, Rhenium and Yttria Additions on the Microstructure of Wide Gap Brazing on IN738," ASME Paper No. GT2007-2712.

[12] Fritsche, B., and Satir-Kolorz, A., 2000, "Repair Brazing of Ni-Base Turbine Blades," Weld. World, **44**(5), pp. 10–14.

[13] Van Esch, H., and Marijnissen, G., 1986, "Braze Repair Techniques," Turbo-

machinery Journal, pp. 29–32.
[14] Demo, W., and Ferrigno, S., 1992, "Brazing Method Helps Repair Aircraft Gas Turbine Nozzles," Process. Adv. Mater., **41**, pp. 43–46.
[15] Ellison, K., Lowden, P., and Liburdi, J., 1992, "Powder Metallurgy Repair of Turbine Components," ASME Paper No. 92-GT-312.
[16] Schoonbaert, S., Huang, X., Yandt, S., and Au, P., 2007, "Brazing and Wide Gap Repair of X-40 Using Ni-Base Alloys," ASME Paper No. GT-2007-27340.
[17] O'Neil, W. M., and Kennedy, A., 2000, "Braze Repairing GT Components: Retrospective, Perspective and Prospective," *20th ASM Heat Treating Conference Proceedings*, Oct. 9–12, pp. 1040–1045.
[18] Juergon, and Malik, M., 1985, "Wide Gap Brazing in Maintenance of Turbine Guide Vanes," DVS-Ber., **98**, pp. 78–82.
[19] Elder, J. E., Thamburaj, R., and Patnaik, P. C., 1989, "Braze Repair of MA754 Aero Gas Turbine Engine Nozzles," ASME Paper No. 89-GT-235.
[20] Lee, J. W., Murray, J. H., and Miller, J. A., 1985, "Development of a New Brazing Technique for Repair of Turbine Engine Components," Weld. J. (Miami, FL, U.S.), October, pp. 18–21.
[21] Nash, P., and Nash, A., 1991, *ASM Handbook*, Vol. 3, Alloy Phase Diagrams, p. 241.
[22] Nash, P., and Jayanth, C., 1991, *ASM Handbook*, Vol. 3, Alloy Phase Diagrams, p. 322.
[23] Miglietti, W., Kearney, J., and Pabon, L., 2001, "Liquid Phase Diffusion Bond Repair of Siemens V84.2, Row 2 Vanes and Alstom Tornado, 2nd Stage Stator Segments," ASME Paper No. 2001-GT-0510.
[24] Miglietti, W., Curtis, R., Hall, B., and Lazarin, C., 2000, "Liquid Phase Diffusion Bond Repair of Westinghouse, W501F, Row 3 Vanes," ASME Paper No. 2000-GT-0339.
[25] Miglietti, W., 2001, "Wide Gap Diffusion Braze Repair of Ni-Based Industrial Turbine Vanes," LOT Conference, Aachen, Germany.